Microearthquake activity around Kueishantao island, offshore northeastern Taiwan: Insights into the volcano–tectonic interactions at the tip of the southern Okinawa Trough

K.I. Konstantinou [a,*], C.-Y. Pan [a], C.-H. Lin [b]

[a] Dept of Earth Sciences, National Central University, 300 Jhongda Rd, Jhongli, 320, Taiwan
[b] Institute of Earth Sciences, Academia Sinica, POB 1–55, Nankang, 115, Taiwan

ARTICLE INFO

ABSTRACT

Kueishantao is a volcanic island located offshore the northeastern coast of Taiwan and lies at the tip of the southern Okinawa Trough which is the back-arc basin of the Ryukyu subduction zone. Its last eruption occurred during the Holocene (~7 ka), hence Kueishantao can be considered as an active volcano. In an effort to better understand how magmatic processes may interact with the regional tectonics, a seismic network was installed in the area during early January 2008. This network consisted of 16 three-component seismometers located both on Kueishantao and the coast of northeastern Taiwan. One year of data was analyzed yielding 425 earthquakes whose P and S arrival times were manually picked and each event was located using a nonlinear probabilistic location method. In order to improve the location accuracy, the minimum 1-D velocity model for this dataset was derived and all earthquakes were relocated using this model. The results show a tight cluster of events near Kueishantao while the remaining earthquakes are scattered between the island and mainland Taiwan. The majority of hypocentral depths range between 2.5 and 10 km where the former depth coincides with the bottom of the shallow sedimentary layer and the latter with the ductile lower crust. Waveforms of the three largest events were also inverted for the determination of their deviatoric and full moment tensor. No statistically significant isotropic component was found, while two of the events can be explained by a double-couple source. The third event exhibited a low frequency content (<10 Hz) and a large non-double-couple component suggesting fluid involvement at its source. A stress inversion of all available focal mechanisms in the area shows that fluid circulation in the upper crust generates a local stress field around Kueishantao facilitating the opening of cracks along the NW–SE direction of regional extension.

© 2013 Elsevier B.V. All rights reserved.

1. Introduction

The Okinawa Trough (OT) is the current back-arc basin of the Ryukyu subduction system and extends from SW Kyushu to NE Taiwan (Fig. 1). The northern and middle areas of the OT have experienced two phases of crustal extension, first in the late Miocene (~10–6 Ma) and then during the Pleistocene (~2–0.1 Ma) (Letouzey and Kimura, 1986; Sibuet et al., 1998). Several geophysical surveys have been conducted in these areas revealing an overall thinned continental crust (~10–15 km), large heat flow anomalies and several active hydrothermal mounds that can be considered as manifestations of strong magmatic activity (Kimura et al., 1988; Klingelhoefer et al., 2009; Lee et al., 1980; Yamano et al., 1989). The southern part of the OT also exhibits strong hydrothermal/magmatic activity, however, geochemical studies indicate that continental rifting is still at an embryonic stage there (Chen et al., 1995; Chung et al., 2000). This observation is also supported by seismic tomography images showing that the area

of the OT closest to Taiwan has a much thicker crust than its middle and northern parts (Wu et al., 2007).

Kueishantao (KST) island lies offshore NE Taiwan in the southern part of the OT and opposite to the Ilan plain (IP). It represents one of the two major volcanic centers in northern Taiwan, the other being the Tatun Volcano Group (Fig. 1). The origin of volcanism at KST is still debated and is either attributed to magmatism due to early stage rifting of the crust (Wang et al., 1999), or to arc volcanism as a result of the Ryukyu subduction (Chung et al., 2000). KST can be considered an active stratovolcano since its last eruption was dated at about 7 ka applying thermoluminescence to a heated siltstone xenolith (Chen et al., 2001). Chiu et al. (2010) have recently studied the geomorphology and volcanic geology of KST using the latest digital terrain model and field mapping techniques. The authors found that volcanic rocks at KST consist of basaltic andesite lava flows, ash fall deposits, pyroclastic flow and lahar deposits as well as hydrothermally altered rocks. The main volcanic edifice lies at the center of the island and has an altitude of 401 m, while there is evidence that part of it has collapsed into the sea during a previous eruptive phase resulting in a large landslide (see Chiu et al., 2010).

* Corresponding author. Tel.: +886 3 4227151x65612; fax: +886 3 4222044.
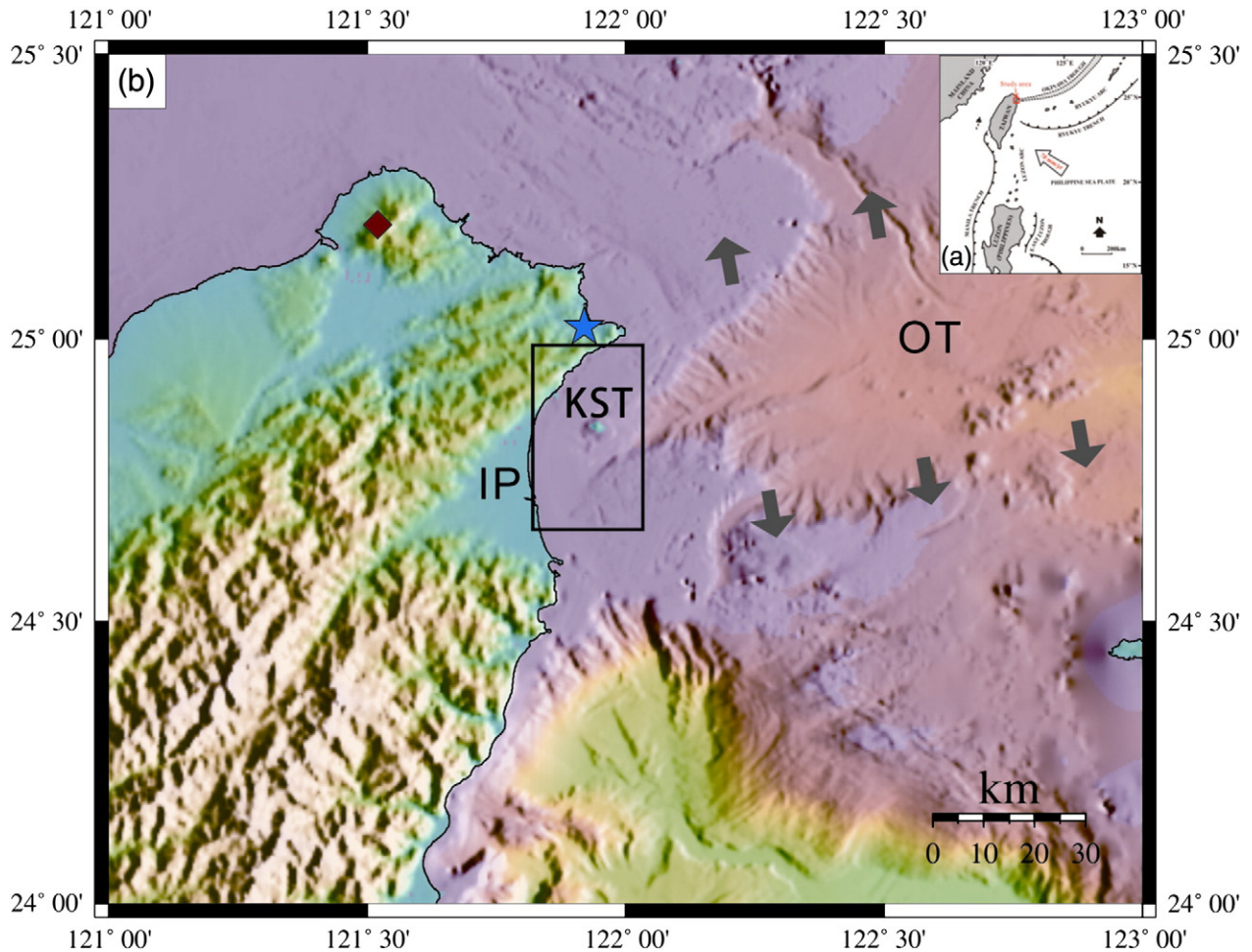E-mail address: kkonst@ncu.edu.tw (K.I. Konstantinou).

Fig. 1. (a) Map showing the location of Taiwan with respect to the regional tectonics that involves the oblique subduction of the Philippines Sea Plate beneath the Eurasian one (after Lai et al., 2009), (b) map of northern Taiwan also showing the offshore bathymetry. The study area is highlighted with a rectangular border around Kueishantao island. The red diamond signifies the location of the Tatun volcano Group which is the other major volcanic center in northern Taiwan. The blue star illustrates the location of the Gongliao nuclear power plant which is under construction. The orientation of extension along the Okinawa Trough is shown with black arrows. KST: Kueishantao, IP: Ilan Plain, OT: Okinawa Trough.

Several submarine hydrothermal vents also exist along the SE coast of KST and continuously emit high-temperature fluids discoloring the seawater around the island.

Geochemical studies have revealed two interesting characteristics for the properties of fumarolic fluids emanating from KST. The first is that gas-bubble samples from submarine vents exhibit very high ^{3}He/^{4}He ratios (~7.3–8.4) which may be the highest reported for hydrothermally active areas in the western Pacific region (Yang et al., 2005). This observation implies that a significant mantle component exists in the gas composition. The second characteristic has to do with the acidity of high-temperature (76–116 °C) hydrothermal fluids that register pH values as low as 1.52 which is among the lowest levels found in similar settings (Chen et al., 2005).

Geophysical or geochemical monitoring of the volcano–hydrothermal system of KST has many practical difficulties. These can mostly be attributed to the fact that the island is uninhabited and difficult to be reached from Taiwan, especially during the winter. Yeh et al. (1989) have utilized analog recordings from a temporary seismic network installed along the Ilan coast for a period of three months, in order to infer seismicity levels around KST. The authors located 275 local earthquakes at depths shallower than 15 km, however, limitations in data quality and in the knowledge of the velocity structure did not allow drawing any major conclusions about the type of seismicity

(volcanic versus tectonic). More recently, Huang et al. (2012) have studied the seismotectonics of NE Taiwan using waveform data from the permanent seismic network operated by Taiwan's Central Weather Bureau (CWB). Their results concerned events with local magnitudes larger than 3.5 and showed a cluster of shallow (<15 km) seismicity around KST. Few focal mechanisms determined by P-wave polarities appeared to be consistent with the regional NW–SE extension expected in the area.

In this paper we make use of high-quality waveform data in order to investigate the microearthquake activity around KST and understand the relationship between the volcano and regional tectonics in this area. First, we give a description of the available data and the temporal distribution of earthquake activity; then we obtain initial locations and invert the observed travel times in order to establish a minimum 1-D velocity model. Accurate absolute locations are derived using this well-calibrated model along with a probabilistic nonlinear location method. The waveforms of the largest events in our dataset are also inverted for the purpose of determining their deviatoric and full moment tensors in an effort to check whether fluid-related processes are involved in their generation. The dominant stress field around KST is also investigated through the stress inversion of all available focal mechanisms. Finally, we close with a discussion and synthesis of the results and their implications for future monitoring efforts at KST island.

2. Data collection and analysis

In early January 2008 the Institute of Earth Sciences, Academia Sinica installed a temporary seismic network for the purpose of monitoring the earthquake activity around KST island (Fig. 2 and Table 1). This network consisted of 16 three-component instruments of which 12 of them were equipped with Guralp CMG-6TD and the other 4 with Lennartz LE3D-Lite short-period sensors. All stations were recording continuously at a sampling interval of 100 samples per second and absolute timing was provided by GPS receivers. Twelve stations were installed along the Ilan coast taking advantage of its curved shape (thus minimizing the azimuthal gap), while the remaining four were installed on KST in order to be as close as possible to the potential seismic sources. In this work we focus on the period starting from the installation of the network in January 2008 until the end of December 2008, covering almost one year worth of data.

The starting point of our analysis was to isolate local from the regional or teleseismic events that have been recorded by the seismic network. Teleseismic events were identified after checking the NEIC (National Earthquake Information Center, US Geological Survey) database and regional events after consulting the CWB catalog. This procedure yielded a total of 1087 local earthquake events that were manually picked only if they conformed to the following criteria: (a) at least 5 stations recorded the event with a high signal-to-noise ratio, (b) an S-phase was clearly recorded by at least 2 stations, and

Table 1
List of seismic stations deployed at KST island and the Ilan coast for the period between January and December 2008.

Station	Lon (°E)	Lat (°N)	Elev (m)	Sensor type
IL01	122.00177	25.00785	92	CMG-6TD
IL02	121.92467	24.97429	110	CMG-6TD
IL03	121.88192	24.94345	308	LE3D-Lite
IL04	121.84703	24.90052	179	CMG-6TD
IL05	121.80643	24.83315	2	CMG-6TD
IL06	121.80930	24.77234	11	LE3D-Lite
IL07	121.80009	24.74912	11	CMG-6TD
IL08	121.82978	24.66531	3	CMG-6TD
IL09	121.86324	24.60932	2	CMG-6TD
IL10	121.95608	24.84671	130	CMG-6TD
IL11	121.94860	24.84859	40	CMG-6TD
IL12	121.94202	24.83846	20	CMG-6TD
IL13	121.95608	24.84671	130	LE3D-Lite
IL14	121.75522	24.83742	130	LE3D-Lite
IL15	121.70988	24.78869	176	CMG-6TD
IL16	121.62503	24.73384	305	CMG-6TD

(c) at least one of the 5 stations was located on KST island. After enforcing all of these criteria 425 local earthquakes eventually remained. Fig. 3 shows the temporal distribution for every month of all events, both the ones included in the final dataset and those that did not conform to our criteria. It should be noted that a large number of picked events either were located outside the network, or they were recorded by only three stations and were not included in the
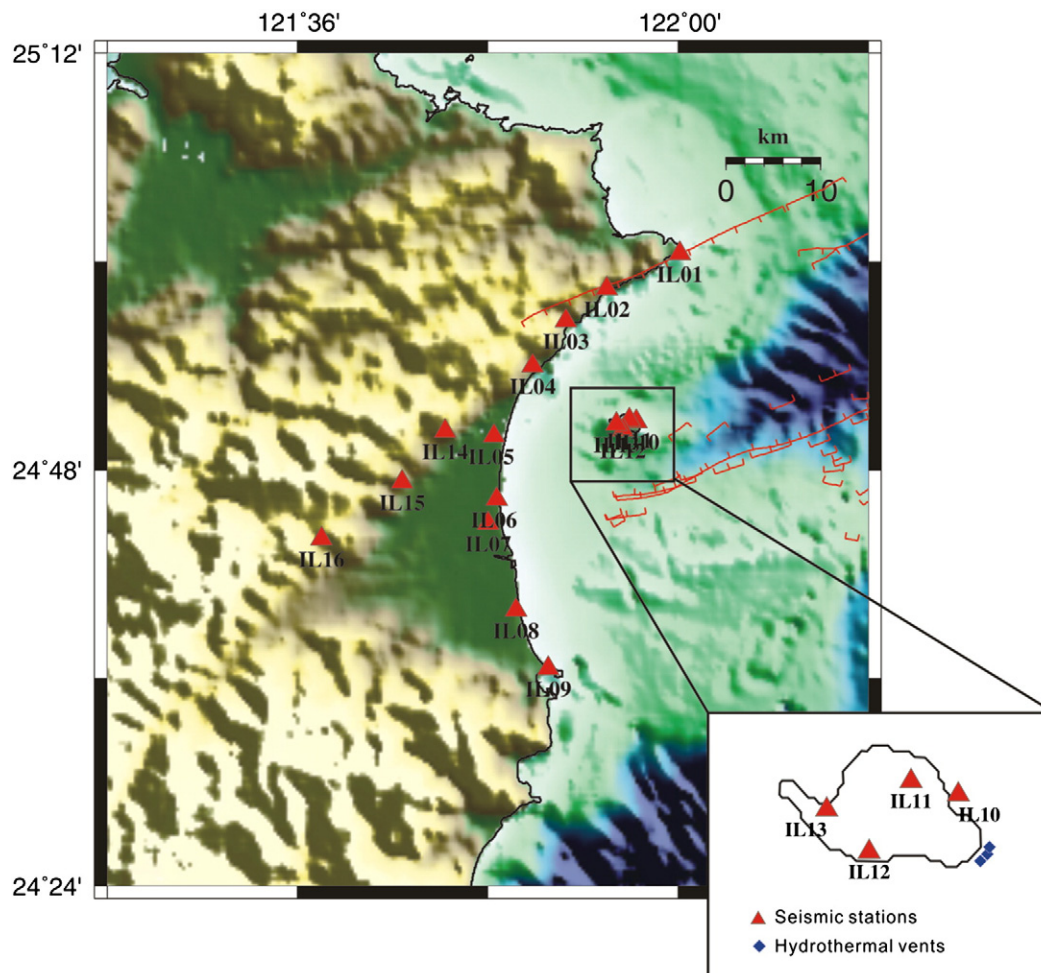

Fig. 2. Map showing the locations of the seismic stations installed on the Ilan plain and those on Kueishantao island (inset). Also shown in the inset map are the locations of the submarine hydrothermal vents mapped by Chen et al. (2005). Active fault lines shown in red are taken from the database of Deffontaines et al. (2001).
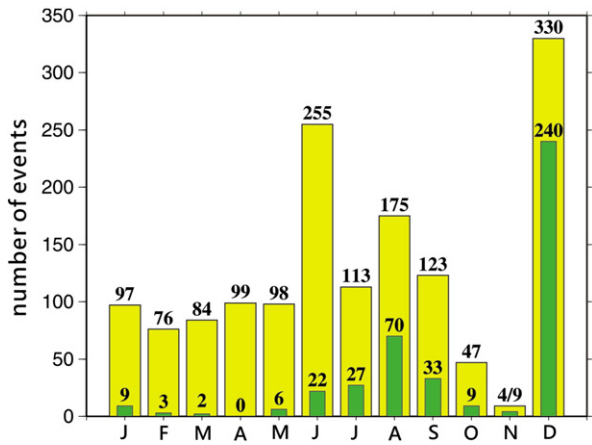
Fig. 3. Histogram depicting the temporal distribution of local seismic events that were isolated and analyzed in this study. The yellow bars represent all local events isolated from regional or teleseismic signals during the study period. The green bars represent events that passed the selection criteria and were included in the final dataset (see text for more details).

final dataset. During June, August and December the seismic activity exhibits prominent peaks, while during the remaining period an average of about 100 events per month is registered. This level of seismic activity is far higher than the one observed in the Tatun Volcano Group (Konstantinou et al., 2007; Rontogianni et al., 2012).

In addition to picking arrival times, we also conducted a spectral analysis of these events in order to investigate possible differences in their frequency content. Propagation effects may be quite severe in volcanic areas and can potentially distort features related to anomalous source effects if the source-receiver distance is large and/or the signal is recorded by only a few stations. For this purpose we made use of all available stations and focused particularly on waveforms recorded on KST. All of the events contained in the final dataset exhibit both clear P- and S-phases and the majority show high frequency (>10 Hz) content (Fig. 4a) which can be considered typical for earthquakes caused by shear failure of rock. However, 19 events showed an abnormally low frequency content with the highest energy occurring at or below 5 Hz (Fig. 4b), indicating source characteristics that may deviate from the shear faulting model. This point will be investigated further in the section dealing with the source inversion.
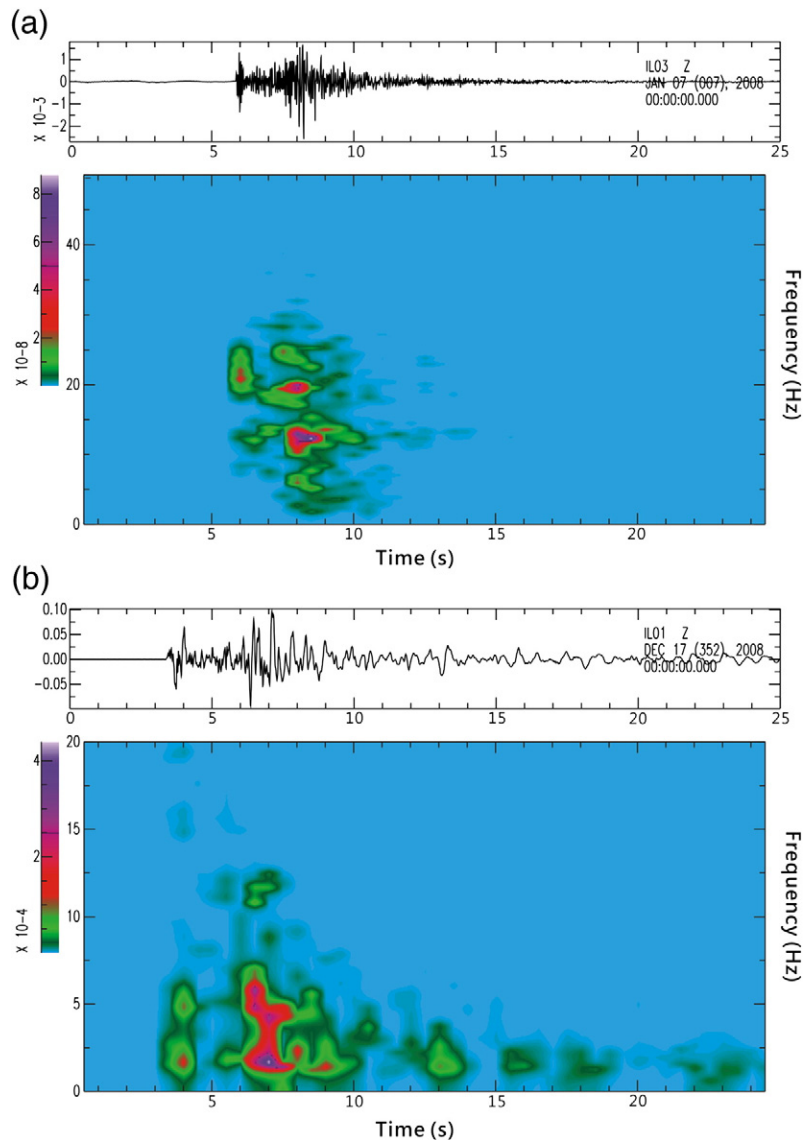

Fig. 4. (a) Vertical velocity waveform and corresponding spectrogram for a high-frequency event that occurred in January 7, 2008. The spectrogram was calculated for a 0.5 s window and 50% overlap using the technique of Goldstein and Minner (1996), (b) vertical velocity waveform and corresponding spectrogram for a low-frequency event that occurred in December 17, 2008 and was the largest event (M_L 4.4) to be recorded during the period of our study. The spectrogram was calculated in the same way as in (a).
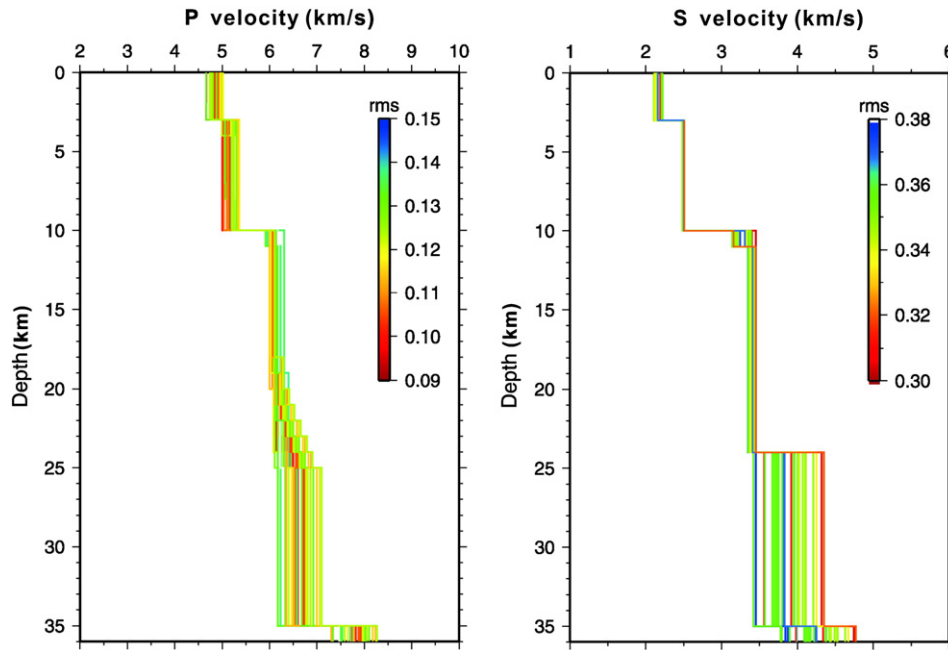
Fig. 5. Left panel: distribution as a function of depth for P-wave velocity of the best 30 models that were used as input to VELEST. The color of the line for each model corresponds to its root mean square (rms) value determined by VELEST and follows the scale at the right of the plot. Right panel: distribution as a function of depth for S-wave velocity of the best 30 models that were used as input to VELEST. All other symbols are the same as previous.

3. Absolute locations and minimum 1-D velocity model

Initial absolute locations are calculated by using a probabilistic nonlinear method implemented in the freely available software package NONLINLOC (Lomax et al., 2000). Unlike linear approaches, NONLINLOC can be used with 1-D or 3-D velocity models providing comprehensive uncertainty and resolution information represented by a posteriori probability density function (PDF) of model parameters. In brief, the complete probabilistic solution can be expressed as a posteriori PDF if the calculated and observed arrival times are assumed to have Gaussian uncertainties. This assumption allows a direct, analytical evaluation of the PDF for the spatial location and the origin time. A more detailed description of this formulation can be found in Lomax et al. (2000). We compute such a posteriori PDF by utilizing
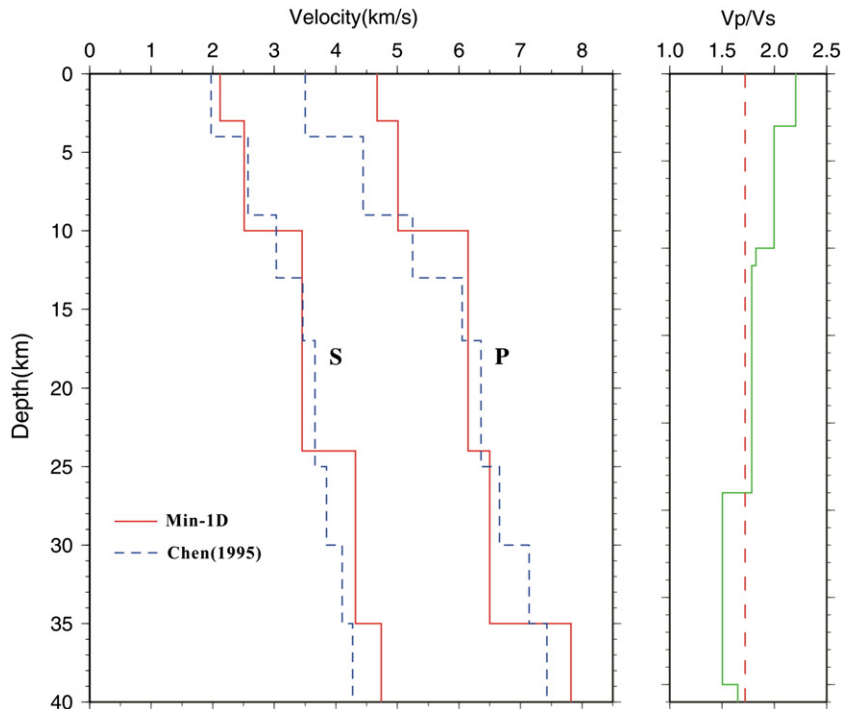

Fig. 6. Left panel: diagram showing the minimum 1-D P- and S-wave velocity model for the study area compared to the model of Chen (1995) which represents an average for the whole Taiwan region. The velocity model is well-constrained only for the upper 25 km. Right panel: the variation as a function of depth of the ratio Vp/Vs stemming from the minimum 1-D model. The red dotted line indicates the value 1.73 which is the average Vp/Vs value for Taiwan (Kim et al., 2005).

Table 2
P- and S-wave station delays determined from the minimum 1-D velocity model inversion using VELEST.

Station	P-delay (s)	S-delay (s)
IL01	0.00	−0.42
IL02	0.20	0.09
IL03	0.33	0.30
IL04	0.37	0.38
IL05	0.44	0.50
IL06	0.37	0.38
IL07	0.37	0.38
IL08	0.33	0.30
IL09	0.20	0.09
IL10	0.08	0.03
IL11	0.08	0.03
IL12	0.10	0.08
IL13	0.10	0.08

the Oct-Tree sampling algorithm that uses recursive subdivision and sampling of cells in 3-D to generate a cascade of sampled cells (Lomax and Curtis, 2001).

In order to obtain initial locations for the events of our dataset, we used the 1-D velocity model suggested by Chen (1995) as an average over the whole of Taiwan, which is also employed by CWB for routine earthquake locations. For the purpose of enhancing the accuracy of our locations, we further estimated a minimum 1-D velocity model for our study area by using the methodology introduced by Kissling et al. (1994) and is implemented in the software code VELEST. The concept of the minimum 1-D velocity model refers to a model that yields the smallest possible uniform error for a set of well-locatable

Fig. 7. Upper panel: distribution of the horizontal difference (in km) between maximum likelihood and Gaussian locations calculated by NONLINLOC for the 425 events of the final dataset. Lower panel: the same for the vertical difference between the two location estimates. The numbers at the upper right hand corner of each plot represent mean and standard deviation of the differences.

events. This is accomplished by inverting P- and S-wave travel times for determining the 1-D velocity structure, earthquake locations and station delays simultaneously. The dataset used for this estimation consists of the 425 events selected previously with 3,565 P-wave and 2,492 S-wave travel times.

We initially chose to invert only the P-wave observations since they provide better spatial sampling and have smaller picking errors than the corresponding S-wave. After obtaining a stable solution for the P-wave velocities we included the S-wave observations in order to obtain the final velocity structure. Several initial models with different layers of thickness and velocities were used in order to avoid being trapped in a local minimum of the solution space. Fig. 5 shows 30 of these initial models that exhibit low values of root mean square (rms) residual. It can be seen that the best P-wave model has an rms value of about 0.09 s while for the corresponding S-wave model this value is much higher, at 0.30 s. Large variations in velocity are evident for depths greater than 25 km and this can be explained if we take into account that the number of rays sampling deeper horizons is limited beyond that depth. This creates the necessity of fixing the P and S velocities deeper than 25 km using values obtained from a seismic tomography study of NE Taiwan (Wu et al., 2007). The final minimum 1-D model and the resulting Vp/Vs ratio can be seen in Fig. 6 while Table 2 lists the station delays obtained. It should be noted that stations IL14, IL15, and IL16 were either too noisy or out of order most of the time and therefore they were not used in the location and minimum 1-D model derivation. One way to test the quality of the velocity model is to examine whether the values of the resulting delays reflect the near-surface geology. Indeed, stations that exhibit small positive values (indicating true velocities lower than those of the 1-D model) are located on volcanoclastic material and sediments. On the other hand, only one station (IL01) located on bedrock exhibits a negative value for the S-wave residual.

Final absolute locations are calculated using NONLINLOC and the minimum 1-D model along with its corresponding station corrections. In order to make an accurate assessment of the errors involved in our location results, we first examined the difference between the resulting maximum likelihood and Gaussian location for each event. The maximum likelihood location corresponds to the minimum misfit point of the complete nonlinear PDF, while the Gaussian one is based on the covariance matrix that is obtained from samples drawn from the PDF. We found that the majority of the events in our dataset exhibit horizontal differences smaller than 0.2 km and vertical differences smaller than 0.5 km (Fig. 7). The small difference of maximum likelihood and Gaussian locations implies a quasi-ellipsoidal PDF exhibiting only a single maximum. NONLINLOC also provides formal estimates of the location error through the dimensions of the confidence ellipsoid and on average these are 0.86 km and 1.53 km for the horizontal and vertical errors respectively. These results show that our picking criteria have successfully screened the original dataset and only well-constrained events have been included in the final catalog.

Having constrained the locations for all events, it is then possible to estimate their local magnitudes (M_L) by measuring on a Wood–Anderson simulated trace their maximum peak-to-peak amplitude on the horizontal components at each station. An attenuation function derived for the Taiwan area and for epicentral distances smaller than 80 km was used in the calculations (for details see Shin, 1993). This procedure resembles the one used by CWB for routine M_L calculation, therefore our magnitude estimates are directly comparable to those found in the CWB catalog. For 10 events that were common in both catalogs, we found that our magnitude values are in good agreement with those published by CWB (differences on average smaller than 0.2 units). The largest magnitude observed during our study period was 4.4 and occurred in December 17, at 19:17 (GMT).
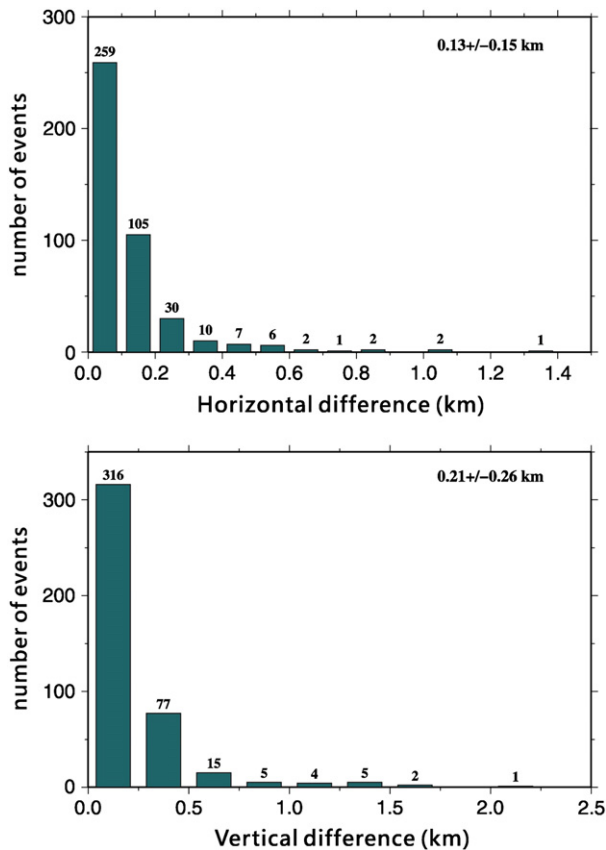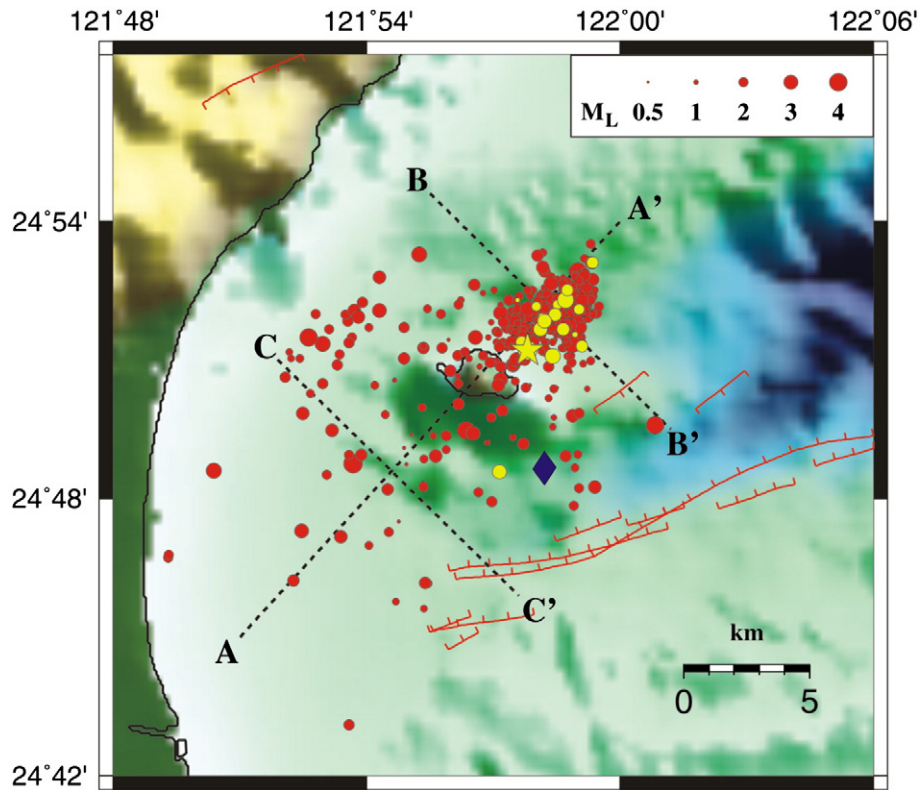
Fig. 8. Map showing the final locations for the 425 events obtained from NONLINLOC by utilizing the minimum 1-D velocity model and station corrections. Red circles represent high-frequency events while yellow circles are low-frequency ones following the December 17 M_L ~4.4 earthquake that is shown as a yellow star. The diamond represents a low-frequency event that occurred before the December 17 large event. Dotted lines show orientations of depth cross-sections. The size of each circle corresponds to local magnitude based on the scale shown at the upper right corner of the plot.

Figs. 8 and 9 show a map of the final 425 event locations we obtained within the study area and three depth cross-sections. It can be seen that one large cluster of events is located very near KST island while the remaining earthquakes are scattered in the area between KST and the Ilan coast. The majority of hypocentral depths lie between 4 and 10 km with very few occurrences of deeper events. These deeper events are not concentrated beneath KST and do not exhibit any anomalously low spectral content. The largest earthquake in our dataset is located at the edge of the observed cluster at a depth of 10 km and this event was followed by numerous smaller earthquakes, hence the large peak in the temporal distribution during December. Some of these earthquakes also have lower spectral content similar to that of the largest earthquake and are located near the base (5–9 km) of the cluster.

4. Moment tensor inversion

The interaction between fluids and solid rock in volcanic or geothermal areas may lead to seismic sources with anomalous ("non-double-couple") characteristics (e.g. Miller et al., 1998). In this context, we investigated the possibility that some of the events in our dataset may exhibit such characteristics through inverting waveforms for moment tensor determination. A necessary condition for applying this methodology to waveform data is that each earthquake is recorded by at least three stations and also exhibits significant energy at periods larger than 10 s. We searched our catalog in order to find events with local magnitudes larger than 3.5 that are recorded by at least three stations with high signal-to-noise ratio at longer periods. This search yielded three events that fulfill these criteria (including the December 17 event). We chose not to include in the inversions data from noisy stations as these would likely degrade the derived moment tensor results.

A linear, time-domain inversion method described by Herrmann and Ammon (2002) was utilized for calculating (a) the deviatoric moment tensor consisting of Compensated Linear Vector Dipole (CLVD) and Double-Couple (DC) components and (b) the full moment tensor with isotropic, CLVD and DC components. The preparation of the waveform data for the inversion involved the deconvolution of the instrument response and rotation of the horizontal components into radial and transverse with respect to the final absolute location of the earthquake. After this the data were filtered in the pass-band 0.03–0.08 Hz using a two-pole Butterworth filter. The choice of this pass-band is a compromise between the necessity of including longer periods in the inversion, thus minimizing the influence of the velocity model and the limited bandwidth of our instruments. Green's functions were calculated for a step of 1 km using the method of wavenumber integration and utilizing the minimum 1-D velocity model determined earlier. The traces were then filtered in exactly the same way and aligned with the observed data according to their arrival times.

It is generally expected that a model with more parameters can fit better the observations than a model with fewer ones. This happens in the case of the deviatoric and full moment tensors where the former needs only five moment tensor elements to be derived versus six for the latter. However, it should be determined whether the model with the extra parameters can fit significantly better in a statistical sense the data. For this purpose we employed an F-test to define which of the two models best represents the seismic source (see for example Dreger et al., 2000). The F-test compares the variances of the misfits for a pair of models and accepts or rejects the null hypothesis that they come from the same distribution at a given confidence level. We found that for a confidence level of 95% the full moment tensor does not fit the data significantly better than the deviatoric moment tensor for all three events. This can be interpreted as an
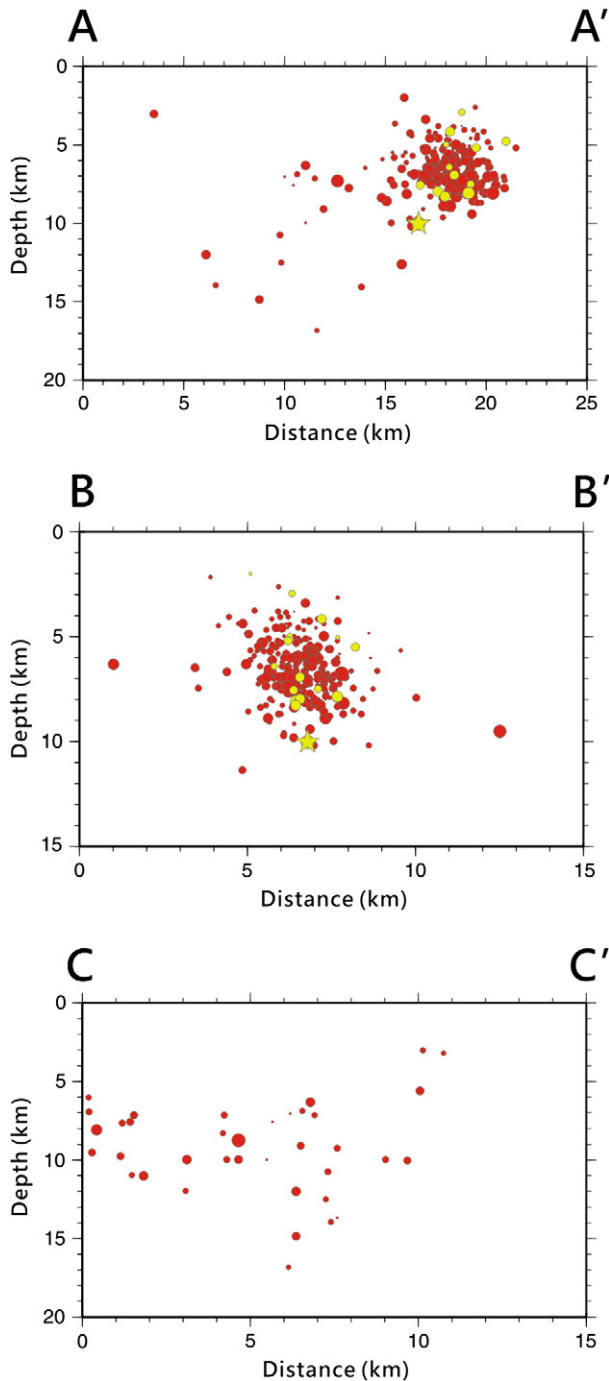
Fig. 9. Depth cross-sections showing the distribution of hypocentral locations along the three profiles shown in Fig. 8. All other symbols are the same as previous.

indication that the isotropic component of these events is statistically insignificant.

Waveforms from five stations were available for inversion of the December 17 earthquake and the results show that the best fit can be obtained at 8 km depth (Fig. 10b). The moment tensor is decomposed into a DC part that amounts to 30% and the CLVD part which is the remaining 70%. The geometry of faulting that represents the DC source shows a focal mechanism with reverse and strike-slip components. On the contrary, the other two events show large DC components indicating source mechanisms that are consistent with shear faulting processes (Fig. 10a,c). It is interesting to note that one of these events exhibits a purely reverse faulting mechanism while the other shows reverse faulting with some strike-slip component. In order to check whether the large

CLVD component present in the moment tensor of the December 17 event is not due to a particular station configuration we performed a jackknife test. In this test the deviatoric moment tensor is determined using all possible combinations of available stations and the variation of CLVD percentage is examined (Fig. 11). It can be seen that when more than three stations are included in the inversion, the amount of the CLVD component becomes stable around 70%. Table 3 gives a summary of the source parameters for the three events where the good agreement can also be seen between the depth derived from the inversion and that from travel time location.

5. Stress tensor inversion

Seismological as well as geodetic observations support the view that the dominant stress field in the area of NE Taiwan is extensional along the NW–SE direction (Huang et al., 2012; Rau et al., 2008). However, the focal mechanisms we obtained for the three largest events in our dataset show a variable component of reverse faulting and this poses the question whether there is a local stress field acting around KST. In order to investigate this possibility we make use of the database of routine CMT solutions determined using waveforms recorded by BATS (Broad-band Array in Taiwan for Seismology, http://bats.earth.sinica.edu.tw/) (Kao et al., 1998). The database covers the period from 1996 up to present and contains solutions for events occurring in and around Taiwan. We search for solutions located in our study area from 1997 up to now with centroid depths shallower than 30 km. The results of this search yielded solutions for 28 events spanning moment magnitudes between 3.4 and 5.0 and showing a range of faulting mechanisms, some of them similar to the ones determined earlier in this study (Fig. 12).

We performed a stress inversion to this set of 31 focal mechanisms (28 from BATS CMTs and 3 derived in this study) in order to elucidate the stress field orientation around KST island. A linear, least-squares inversion method is used where confidence regions for the three stress axes (σ_1, σ_2, σ_3) are estimated by a bootstrap technique (Michael, 1987). The dataset is resampled with replacement 2000 times which is found adequate to produce stable confidence regions up to 95% level (Hardebeck and Hauksson, 2001). The average misfit between the best-fit model and the data in a single inversion is given by β, the angle between the slip direction and the predicted tangential traction on the fault plane. For our inversion results we find that the misfit does not exceed 22° giving an indication that the stress field can be considered approximately homogeneous, if we assume fault plane solution errors between 10° and 20° (Michael, 1991). The results shown in the inset of Fig. 12 reveal a subhorizontal σ_3 axis orientated along NW–SE coinciding with the direction of regional extension. The σ_1 axis is also found to be close to subhorizontal (plunge ~20°) with an orientation perpendicular to that of the extension. It is possible therefore that a local stress field is present around KST which facilitates the opening of cracks along the direction of σ_3 axis and striking subparallel to the σ_1 axis. This stress configuration allows the circulation of fluids in the upper crust as evidenced by the strong hydrothermal activity observed around KST.

6. Discussion

The deep velocity structure of NE Taiwan has been imaged by several tomographic studies previously (Kim et al., 2005; Rau and Wu, 1995; Wu et al., 2007). These studies show that NE Taiwan exhibits a normal crustal thickness (~30–40 km) which is unlike the area eastwards of KST where the crust is substantially thinner (e.g. Klingelhoefer et al., 2009). However, such studies have very little resolution power over small-scale features, therefore there is no information about the possible depth and geometry of the magma chamber beneath KST. Nevertheless, Lin et al. (2004) have performed a tomographic study in this area using a large number of P-/S-wave arrival times obtained from land seismic stations and OBS offshore NE Taiwan. The authors resolved the image of a sausage-shaped

low-velocity body beneath the Ilan plain at depths 25–100 km and speculated that this may be the primary source of fluids feeding the postulated magma chamber beneath KST.

At shallower depths, seismic reflection profiles collected offshore the Ilan coast west of KST, have shown a sedimentary layer up to 2 km thick lying on top of the acoustic basement and several faults buried underneath it (Ku et al., 2009). The anomalously high Vp/Vs ratio (~1.9–2.3) obtained from our minimum 1-D model for the upper 10 km of the study area may be an indication of increased pore-fluid pressure at these depths (Carcione and Cavallini, 2002). It is then likely that the whole of the upper crust around KST is

fractured and saturated by fluids originating from deeper sources, but also from the seawater that fills the pore-spaces of the sedimentary layer. The hypocentral distribution of the observed microseismicity around KST shows a lack of earthquake foci shallower than 2.5 km and at depths greater than 10 km. The former depth correlates with the thickness of the sedimentary layer, while the latter one coincides with the lower crust which appears to be almost aseismic. The ceasing of seismogenesis in the lower crust can probably be explained if we consider the high temperature gradients imposed by the low-velocity body imaged by Lin et al. (2004) that would lead to ductile rather than brittle rock behavior. This interpretation is also
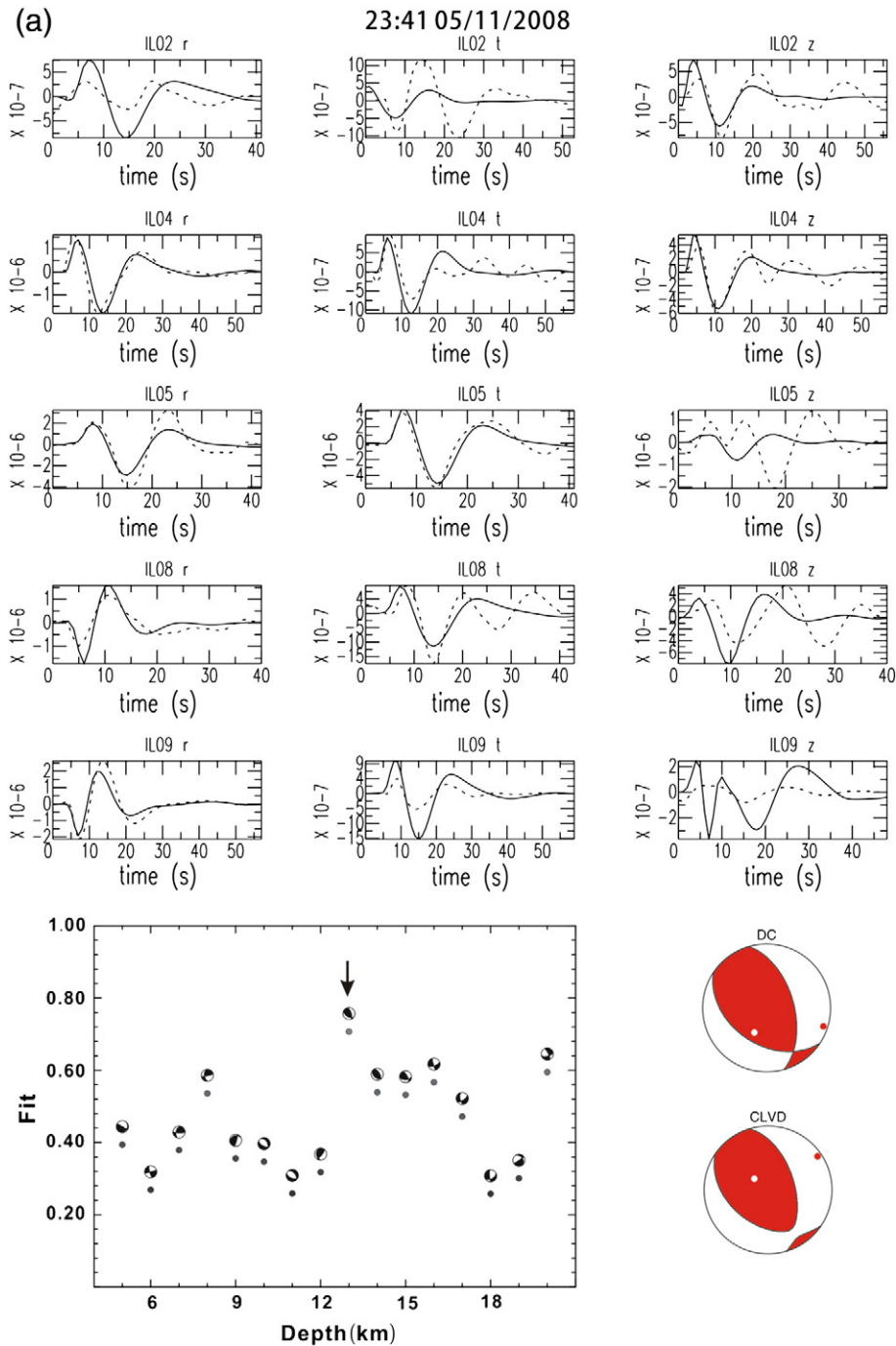

Fig. 10. (a) Deviatoric moment tensor results at 13 km depth for an event that occurred in May 11, 2008. Top panel shows the fit between observed (solid lines) and synthetic (dashed lines) seismograms, while the plot at the bottom shows how the fit varies as a function of depth with the best solution highlighted with an arrow. The two beach balls indicate the double-couple and CLVD components of the best solution, (b) the same for the event that occurred in December 17, 2008, and (c) the same for the event that occurred in December 19, 2008.
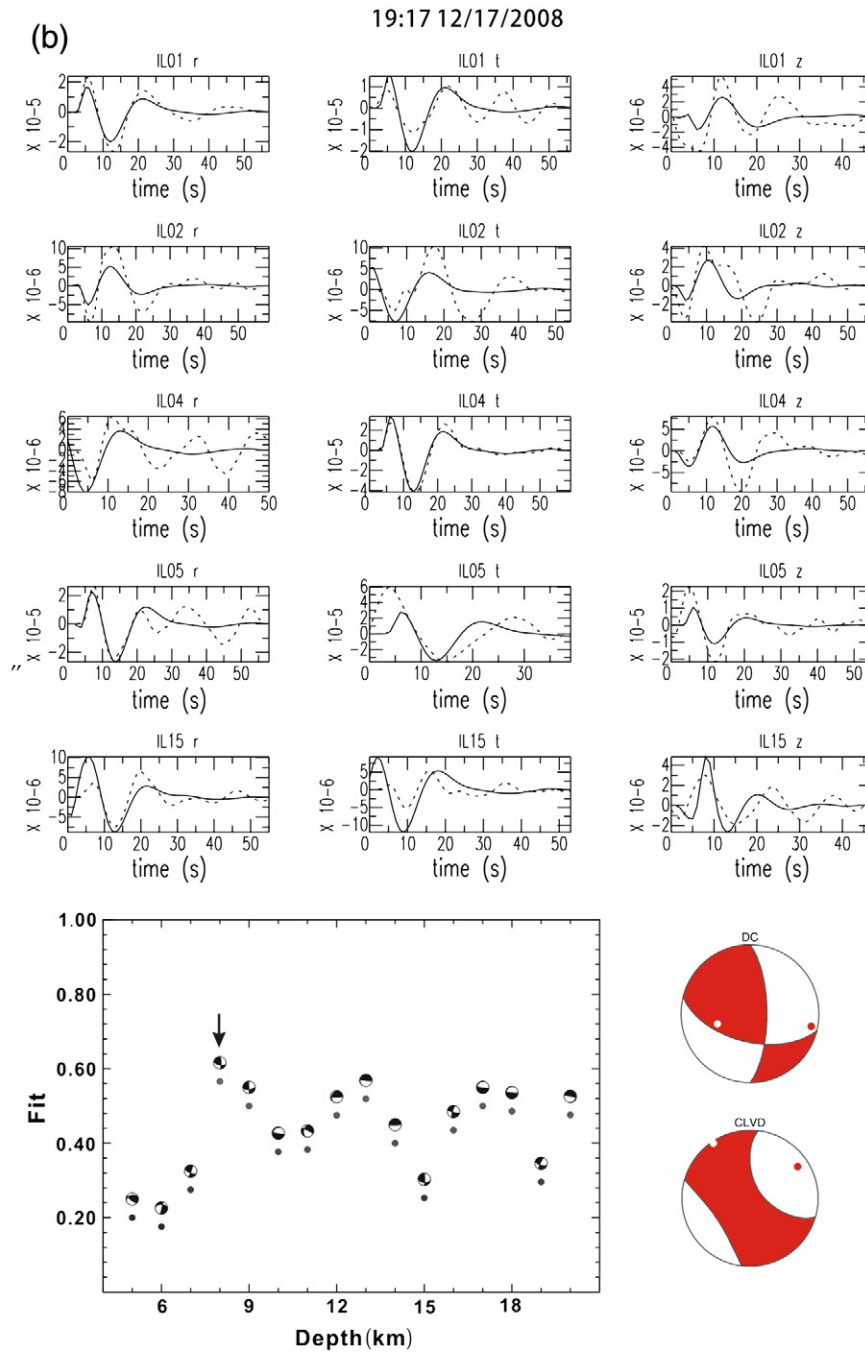
Fig. 10 (continued).

supported by the very high heat flow values (~153 mW m^{-2}) measured at KST and the nearby seafloor (Chiang et al., 2010).

The majority of the earthquakes recorded by our network exhibit clear P- and S-phases and high frequency content implying a physical mechanism related to brittle failure of rock. This is not the case for the December 17 earthquake whose source deviates strongly from the shear faulting model as shown by the moment tensor inversion results. There are two possible interpretations for an event with source characteristics such as a large CLVD but no isotropic component. The first is related to complex rupture geometry, possibly involving fault segments with variable strike such as a ring fault (e.g. Nettles and Ekström, 1998). This explanation seems less likely in our case, as the December 17 event was quite small in magnitude to be the result of rupture complexities and there is no evidence to-date for the existence of a ring fault near KST. The second

interpretation explains the source characteristics by considering a tensile crack coupled with an oblate spheroid magma chamber (see for example Nakamichi et al., 2004). In this configuration, when the crack opens and the chamber shrinks simultaneously, the total moment tensor is equivalent to a large CLVD and smaller DC component with a net volume change equal to zero. Despite the fact that the exact depth of the KST magma chamber is not known, this interpretation seems to be supported by both the large hypocentral depth of this event (~8–10 km) and its location at the base of the cluster of events that followed it. Some of these events also exhibit low-frequency characteristics and may similarly possess anomalous source properties due to fluid involvement.

Fig. 13 synthesizes all the observations analyzed previously and offers a plausible scenario for the interplay between magmatic processes and tectonic forces around KST. The primary source of magmatic fluids
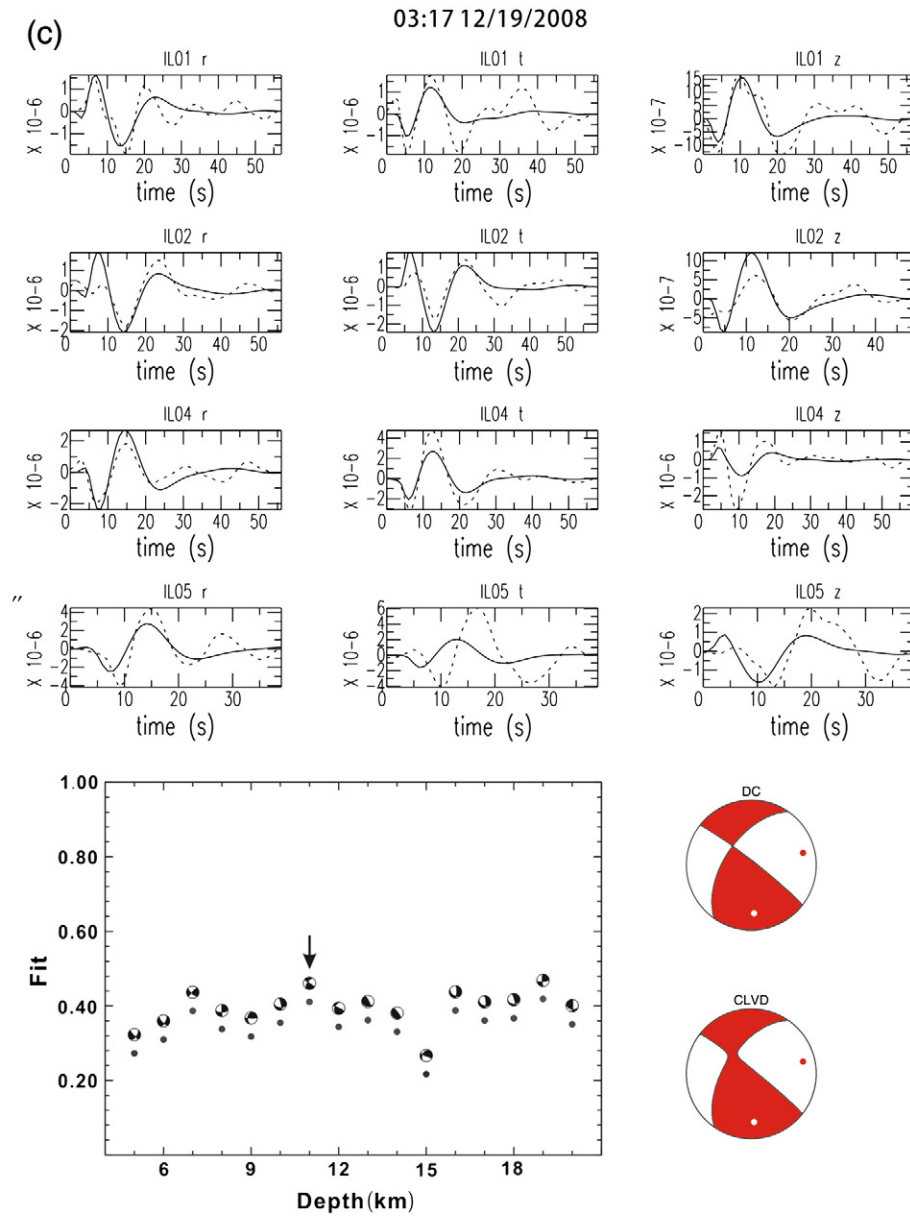
Fig. 10 (continued).

is represented by the low-velocity body imaged by Lin et al. (2004) with its top lying at 25–30 km depth. Fluids in the form of melt or exsolved volatiles feed the postulated magma chamber beneath KST island and also ascend through fractures penetrating the sediments covering the Ilan plain. This is in agreement with geochemical measurements of the air-corrected ratio ^{3}He/^{4}He (R_A) which shows significant mantle contributions in gas-bubbles at KST and in spring water at several locations in the Ilan plain (Yang et al., 2005). In this setting, the December 17 earthquake probably signifies fluid injection from the magma chamber to shallower depths through a system of cracks that serve as the conduitssupplying with fluids the hydrothermal system of the volcano. Horizontal compressive stresses act in concert with the regional extensional stress to open cracks and transfer the fluids at shallower levels within the upper crust.

The findings of this study stress the importance of monitoring KST as a means of mitigating the hazards from future eruptive activity. Such hazards do not only include those purely related to volcanic activity (e.g. pyroclastic flows, ash fall, ballistic projectiles), but also the ones generated by secondary processes like landslide-induced
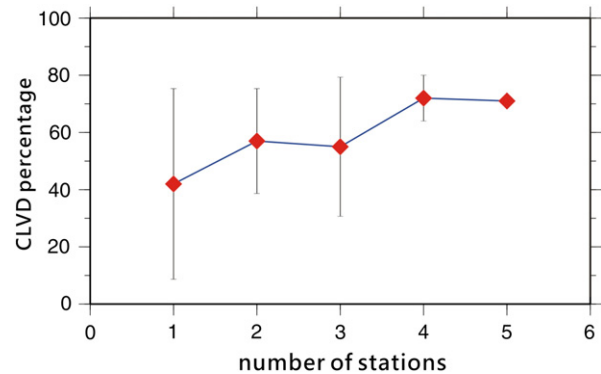

Fig. 11. Diagram showing the variation of the CLVD percentage of the December 17 earthquake as a function of the number of stations included in the inversion. The red diamonds show the average CLVD percentage of all possible station combinations, while the error bars represent the standard deviations.

Table 3

Source parameters of the three events whose moment tensor solutions were determined in this study. The column H signifies the hypocentral depth estimated by NONLINLOC, while the column MT represents the depth that the moment tensor solution showed the best fit.

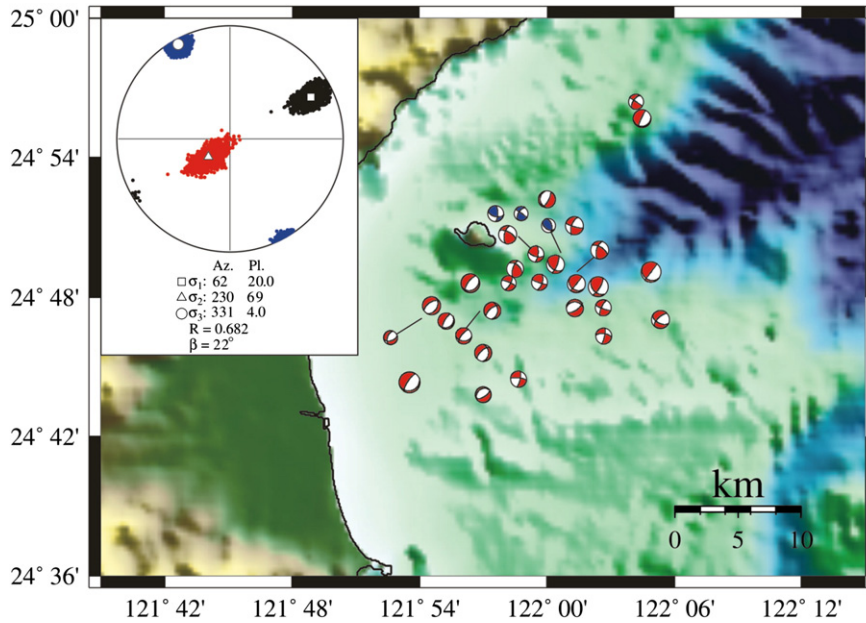|			Plane1			Plane2						
OT(2008)	Lat	Lon	φ_1	δ_1	ξ_1	φ_2	δ_2	ξ_2	Mw	Mo (dyn-cm)	H (km)	MT (km)
20080511	24.83	122.01	344	55	116	123	42	57	3.4	0.161e + 22	9.5	13
20081217	24.86	121.96	0	70	144	104	56	25	3.8	0.694e + 22	10	8
20081219	24.86	121.98	305	87	32	213	58	177	3.4	1.38e + 21	6.8	11

Fig. 12. Map showing the spatial distribution of all available focal mechanism solutions for the area around KST island. Red beach balls represent CMT solutions derived from the BATS database for events shallower than 30 km, while blue ones correspond to the three moment tensor solutions determined in this study. The inset at the upper left hand corner shows the results of stress inversion using this set of 31 focal mechanisms. The dots define the 95% confidence region of each stress axis. Az: azimuth, Pl: plunge, R is a value given by $\sigma_2-\sigma_3/\sigma_1-\sigma_3$ and indicates relative stress magnitude.
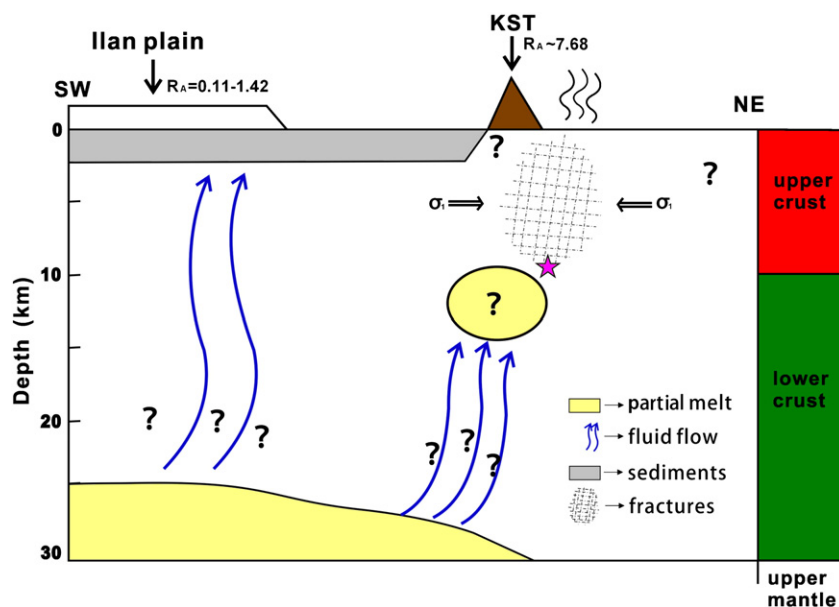

Fig. 13. Schematic cartoon illustrating the possible configuration of the volcano–hydrothermal system beneath KST and its relationship with the regional geology and tectonics (see text for more details). The purple star signifies the hypocentral location of the December 17 earthquake. The symbol R_A refers to the Helium isotope ratio values determined by Yang et al. (2005) from samples taken at KST and the Ilan plain.

tsunami. The latter hazard may potentially be the most dangerous since the Ilan area is a densely populated flat plain, setting a suitable ground for deep penetration of the tsunami waves inland. Additionally, the Gongliao nuclear power plant is currently under construction along the coast (cf Fig. 1) and any issues regarding its safety in the case of such a tsunami should be addressed, especially in the aftermath of the Fukushima disaster. Therefore a coordinated multi-disciplinary (geophysical, geodetic, geochemical) monitoring program is needed in order to achieve effective hazard mitigation.

References

Carcione, J.M., Cavallini, F., 2002. Poisson's ratio at high pore pressure. Geophysical Prospecting 50, 97–106.
Chen, Y.L., 1995. Three-dimensional velocity structure and kinematic analysis in the Taiwan area, PhD thesis, National Central University, Jhongli, Taiwan.
Chen, C.-H., Lee, T., Shieh, Y.-N., Chen, C.-H., Hsu, W.-Y., 1995. Magmatism at the onset of back-arc spreading in the Okinawa Trough. Journal of Volcanology and Geothermal Research 69, 313–322.
Chen, Y.-G., Wu, W.-S., Liu, T.-K., Chen, C.-H., 2001. A date for volcanic eruption inferred from siltstone xenolith. Quaternary Science Reviews 20, 869–873.
Chen, C.-T.A., Zeng, Z., Kuo, F.-W., Yang, T.-F., Wang, B.-J., Tu, Y.-Y., 2005. Tide-influenced acidic hydrothermal system offshore NE Taiwan, Chem. Geology 224, 69–81. http://dx.doi.org/10.1016/j.chemgeo.2005.07.022.
Chiang, H.-T., Shyu, C.-T., Chang, H.-I., Tsao, S., Chen, C.-X., 2010. Geothermal monitoring of Kueishantao island offshore of northeastern Taiwan. Terrestrial, Atmospheric and Oceanic Sciences 21, 563–573. http://dx.doi.org/10.3319/TAO.2009.11.02.01(TH).
Chiu, C.-L., Song, S.-R., Hsieh, Y.-C., Chen, C.-X., 2010. Volcanic characteristics of Kueishantao in Northeast Taiwan and its implications. Terrestrial, Atmospheric and Oceanic Sciences 21, 575–585. http://dx.doi.org/10.3319/TAO.2010.02.22.02(TH).
Chung, S.-L., Wang, S.-L., Shinjo, R., Lee, C.-S., Chen, C.-H., 2000. Initiation of arc magmatism in an embryonic continental rifting zone of the southernmost part of Okinawa Trough. Terra Nova 12, 225–230.
Deffontaines, B., et al., 2001. Preliminary neotectonic map of onshore-offshore Taiwan. Terrestrial, Atmospheric and Oceanic Sciences (Suppl. Issue), 339–349.
Dreger, D., Tkalcic, H., Johnston, M., 2000. Dilational processes accompanying earthquakes in Long Valley caldera. Science 288, 122–125. http://dx.doi.org/10.1126/science.288.5463.122.
Goldstein, P., Minner, L., 1996. SAC2000: seismic signal processing and analysis tools for the 21st century. Seismological Research Letters 67, 39.
Hardebeck, J.L., Hauksson, E., 2001. Stress orientations obtained from earthquake focal mechanisms: what are appropriate uncertainty estimates? Bulletin of the Seismological Society of America 91, 250–262.
Herrmann, R.B., Ammon, C.J., 2002. Computer programs in seismology — source inversions: user's manual, report. St Louis University, St Louis Mo.
Huang, H.-H., Shyu, J.B.H., Wu, Y.-M., Chang, C.-H., Chen, Y.-G., 2012. Seismotectonics of northeastern Taiwan: kinematics of the transition from waning collision to subduction and postcollisional extension. Journal of Geophysical Research 117, B01313. http://dx.doi.org/10.1029/2011JB008852.
Kao, H., Jian, P.-R., Ma, K.-F., Huang, B.-S., Liu, C., 1998. Moment tensor inversion for offshore earthquakes east of Taiwan and their implications for regional collision. Geophysical Research Letters 25, 3619–3622.
Kim, K.H., Chiu, J.-M., Pujol, J., Chen, K.-C., Huang, B.-S., Yeh, Y.-H., Peng, S., 2005. Three-dimensional Vp and Vs structural models associated with the active subduction and collision tectonics in the Taiwan region. Geophysical Journal International 162, 204–220. http://dx.doi.org/10.1111/j.1365-246X.2005.02657.x.
Kimura, M., Uyeda, S., Kato, Y., Tanaka, T., Yamano, M., Gamo, T., Sakai, H., Kato, S., Izawa, E., Oomori, T., 1988. Active hydrothermal mounds in the Okinawa Trough backarc basin, Japan. Tectonophysics 145, 319–324.

Kissling, E., Ellsworth, W.-L., Eberhart-Phillips, D., Kradolfer, U., 1994. Initial reference models in local earthquake tomography. Journal of Geophysical Research 99, 19635–19646.
Klingelhoefer, F., Lee, C.-S., Lin, J.-Y., Sibuet, J.-C., 2009. Structure of the southernmost Okinawa Trough from reflection and wide-angle seismic data. Tectonophysics 466, 281–288. http://dx.doi.org/10.1016/j.tecto.2007.11.031.
Konstantinou, K.I., Lin, C.-H., Liang, W.-T., 2007. Seismicity characteristics of a potentially active Quaternary volcano: the Tatun Volcano Group, northern Taiwan. Journal of Volcanology and Geothermal Research 160, 300–318. http://dx.doi.org/10.1016/j.jvolgeores.2006.09.009.
Ku, C.-Y., Hsu, S.-K., Sibuet, J.-C., Tsai, C.-H., 2009. The neotectonic structure of the southwestern tip of the Okinawa Trough. Terrestrial, Atmospheric and Oceanic Sciences 20, 749–759. http://dx.doi.org/10.3319/TAO.2008.09.01.01(Oc).
Lai, K.Y., Chen, Y.G., Wu, Y.M., Avouac, J.P., Kuo, Y.T., Wang, Y., Chang, C.H., Lin, K.C., 2009. The 2005 Ilan earthquake doublet and seismic crisis in northeastern Taiwan: evidence for dike intrusion associated with on-land propagation of the Okinawa Trough. Geophysical Journal International 179, 678–686. http://dx.doi.org/10.1111/j.1365-246X.2009.04307.x.
Lee, C.-S., Shor, G., Bibee, L.D., Lu, R.S., Hilde, T.W.C., 1980. Okinawa Trough: origin of a back-arc basin. Marine Geology 35, 219–241.
Letouzey, J., Kimura, M., 1986. The Okinawa Trough genesis, structure and evolution of a backarc basin developed in a continent. Marine and Petroleum Geology 2, 111–130.
Lin, J.-Y., Hsu, S.-K., Sibuet, J.-C., 2004. Melting features along the western Ryukyu slab edge (northeast Taiwan): tomographic evidence. Journal of Geophysical Research 109, B12402. http://dx.doi.org/10.1029/2004JB003260.
Lomax, A., Curtis, A., 2001. Fast, probabilistic earthquake location in 3D models using Oct-tree importance sampling. Geophysical Research Abstracts 3.
Lomax, A., Virieux, J., Volant, P., Berge-Thierry, C., 2000. Probabilistic earthquake location in 3D and layered models. In: Thurber, Rabinowitz (Ed.), Advances in Seismic Event Location, pp. 101–134.
Michael, A.J., 1987. Use of focal mechanisms to determine stress: a control study. Journal of Geophysical Research 92, 357–368.
Michael, A.J., 1991. Spatial variations in stress within the 1987 Whittier Narrows, California, aftershock sequence: new techniques and results. Journal of Geophysical Research 96, 6303–6319.
Miller, A.D., Foulger, G.R., Julian, B.R., 1998. Non-double-couple earthquakes 2. Observations. Reviews of Geophysics 36, 551–568.
Nakamichi, H., Hamaguchi, H., Tanaka, S., Ueki, S., Nishimura, T., Hasegawa, A., 2004. Source mechanisms of deep and intermediate-depth low-frequency earthquakes beneath Iwate volcano, northeastern Japan. Geophysical Journal International 154, 811–828.
Nettles, M., Ekström, G., 1998. Faulting mechanism of anomalous earthquakes near Bardarbunga volcano, Iceland. Journal of Geophysical Research 103, 17973–17983.
Rau, R.J., Wu, F.-T., 1995. Tomographic imaging of lithospheric structures under Taiwan, Earth Planet. Science Letters 133, 517–532.
Rau, R.-J., Ching, K.-E., Hu, J.-C., Lee, J.-C., 2008. Crustal deformation and block kinematics in transition from collision to subduction: global positioning system measurements in northern Taiwan, 1995–2005. Journal of Geophysical Research 113, B09404. http://dx.doi.org/10.1029/2007JB005414.
Rontogianni, S., Konstantinou, K.I., Lin, C.-H., 2012. Multi-parametric investigation of the volcano–hydrothermal system at Tatun Volcano Group, Northern Taiwan. Natural Hazards and Earth System Sciences 12, 2259–2270. http://dx.doi.org/10.5194/nhess-12-2259-2012.
Shin, T.C., 1993. The calculation of local magnitude from the simulated Wood–Anderson seismograms of the short-period seismograms in the Taiwan area. Terrestrial, Atmospheric and Oceanic Sciences 4, 155–170.
Sibuet, J.-C., et al., 1998. Okinawa Trough back-arc basin: early tectonic and magmatic evolution. Journal of Geophysical Research 103, 30245–30267.
Wang, K.-L., Chung, S.-L., Chen, C.-H., et al., 1999. Post-collisional magmatism around northern Taiwan and its relation with opening of the Okinawa Trough. Tectonophysics 308, 363–376.
Wu, Y.-M., Chang, C.-H., Zhao, L., Shyu, J.B.H., Chen, Y.-G., Sieh, K., Avouac, J.-P., 2007. Seismic tomography of Taiwan: improved constraints from a dense network of strong stations. Journal of Geophysical Research 112, B08312. http://dx.doi.org/10.1029/2007JB004983.
Yamano, M., Uyeda, S., Foucher, J.-P., Sibuet, J.-C., 1989. Heat flow anomaly in the middle Okinawa Trough. Tectonophysics 159, 307–318.
Yang, T.F., Lan, T.F., Lee, H.-F., Fu, C.-C., Chuang, P.-C., Lo, C.-H., Chen, C.-H., Chen, C.-T.A., Lee, C.-S., 2005. Gas compositions and helium isotopic ratios of fluid samples around Kueishantao, NE offshore Taiwan and its tectonic implications. Geochemical Journal 39, 469–480.
Yeh, Y.-H., Lin, C.-H., Roecker, S.W., 1989. A study of upper crustal structures beneath northeastern Taiwan: possible evidence of the western extension of Okinawa Trough. Proceedings of the Geological Society of China 32, 139–156.